



**HAL**  
open science

## Low dispersion spectra of lunar impact flashes in 2018 Geminids

Masahisa Yanagisawa, Yuki Uchida, Seiya Kurihara, Shinsuke Abe, Ryota Fuse, Satoshi Tanaka, Keisuke Onodera, Fumi Yoshida, Hsin-Chang Chi, Zhong-Yi Lin, et al.

► **To cite this version:**

Masahisa Yanagisawa, Yuki Uchida, Seiya Kurihara, Shinsuke Abe, Ryota Fuse, et al.. Low dispersion spectra of lunar impact flashes in 2018 Geminids. *Planetary and Space Science*, 2021, 195, pp.105131. 10.1016/j.pss.2020.105131 . insu-03439588

**HAL Id: insu-03439588**

**<https://insu.hal.science/insu-03439588>**

Submitted on 22 Nov 2021

**HAL** is a multi-disciplinary open access archive for the deposit and dissemination of scientific research documents, whether they are published or not. The documents may come from teaching and research institutions in France or abroad, or from public or private research centers.

L'archive ouverte pluridisciplinaire **HAL**, est destinée au dépôt et à la diffusion de documents scientifiques de niveau recherche, publiés ou non, émanant des établissements d'enseignement et de recherche français ou étrangers, des laboratoires publics ou privés.



Distributed under a Creative Commons Attribution - NonCommercial - NoDerivatives 4.0 International License



## Low dispersion spectra of lunar impact flashes in 2018 Geminids

Masahisa Yanagisawa<sup>a,\*</sup>, Yuki Uchida<sup>a</sup>, Seiya Kurihara<sup>a</sup>, Shinsuke Abe<sup>b</sup>, Ryota Fuse<sup>b</sup>, Satoshi Tanaka<sup>c</sup>, Keisuke Onodera<sup>c,d</sup>, Fumi Yoshida<sup>e</sup>, Hsin-Chang Chi<sup>f</sup>, Zhong-Yi Lin<sup>g</sup>, Jim Lee<sup>h</sup>, Taichi Kawamura<sup>i</sup>, Ryuhei Yamada<sup>j</sup>

<sup>a</sup> Department of Engineering Science, The University of Electro-Communications, Japan

<sup>b</sup> Department of Aerospace Engineering, Nihon Univ, Japan

<sup>c</sup> Institute of Space and Astronautical Science, Japan Aerospace Exploration Agency, Japan

<sup>d</sup> School of Physical Sciences, Department of Space and Astronautical Science, The Graduate University for Advanced Studies (SOKENDAI), Japan

<sup>e</sup> Planetary Exploration Research Center, Chiba Institute of Technology, Japan

<sup>f</sup> Department of Physics, National Dong Hwa University, Taiwan

<sup>g</sup> Graduate Institute of Astronomy, National Central University, Taiwan

<sup>h</sup> Taipei Astronomical Museum, Taiwan

<sup>i</sup> Institut de Physique du Globe de Paris, University of Paris Diderot, France

<sup>j</sup> School of Computer Science and Engineering, Aizu University, Japan



### ARTICLE INFO

#### Keywords:

Visible and near-infrared spectrum  
Lunar impact flash  
Geminids

### ABSTRACT

Lunar impact flashes have been observed at collisions of meteoroids against the non-sunlit lunar surface at speeds exceeding  $10 \text{ km s}^{-1}$ . We detected 13 flash candidates between 6.2 and 9.9 in R-magnitude on December 15, 2018 during the Geminids meteor activity. Two or three observatories confirmed eleven of them. We obtained their spectra in the wavelength range between 400 and 870 nm. They are continuous and red, with best-fitted single blackbody spectra indicating the temperatures of about 2000–4000 K. The temperatures for a few successive movie frames at 16 ms or 25 ms intervals decrease with time. Incandescent ejecta, consisting of melt droplets or dust, and the radiant floor of an impact crater could be the source of these flashes, except for the initial stages. At the beginning of some flashes, we found an excess of fluxes at short wavelengths of less than about 600 nm. The composites of two blackbody spectra may fit the spectra better where their temperatures are about 2000 K and 6000 K. The contribution of a high-temperature vapor plume, generated at the very beginnings of the impact phenomena, could be important.

### 1. Introduction

At collisions in the solar system, there are many cases where the collisions occur at speeds exceeding  $10 \text{ km s}^{-1}$ , which almost cannot be reproduced in laboratory experiments (e.g., Kurosawa et al., 2012a). In such a collision, melting, evaporation, and ionization of silicates occur, which do not occur at speed lower than this. Understanding of high-speed collisions accompanying such processes is an essential issue in planetary sciences. Not only numerical simulations (e.g., Nemtchinov et al., 1998a; Nemtchinov et al., 1998; Artemieva et al., 2000) but also many laboratory experiments have been conducted to reveal the nature of impact vaporizations (e.g., Schultz 1996; Sugita et al., 2003; Schultz and Eberhardy 2015). They use proxy target materials such as dolomite or calcite that evaporate at lower impact velocities (Kurosawa et al., 2012b). The

knowledge obtained through these experiments was successfully applied to interpreting the phenomena at the spacecraft's impact on Comet 9P/Tempel 1 at  $10 \text{ km s}^{-1}$  (Deep Impact). It was used to derive the surface properties of the comet (Schultz et al., 2007; Ernst and Schultz 2007). However, our knowledge about the impact phenomena at much higher velocities is still limited. We can approach this problem from the observation of lunar impact flashes.

Spectral information is important to study the mechanism of lunar impact flashes. Madio et al. (2018) observed a flash on March 25, 2015 at both near-infrared and visible wavelengths in their MIDAS project (Madio et al., 2019a). Its V-band magnitude was about 7 at the beginning, then the brightness decreased with time, and their cameras recorded the flash for about 0.2 s. They assumed blackbody radiation and estimated its temperature to be about 4000 K at the initial phase,

\* Corresponding author. 5-37-6-202 Tsurumaki, Tama-shi, Tokyo, 206-0034, Japan.

E-mail address: [yanagi.uec@gmail.com](mailto:yanagi.uec@gmail.com) (M. Yanagisawa).

followed by temperatures of about 3200 K after the peak of its brightness. Unfortunately, the exposure timings of their two cameras, one for the visible and the other for the near-infrared wavelengths, were not synchronized. Each frame is time-stamped with an accuracy of 0.01 s. However, the difference of the exposure timings less than 0.01 s could lead to a non-negligible error in their temperature derivation because the time constant of the brightness variation of lunar flashes is generally not so long, especially at their beginnings.

A lunar monitoring project NELIOTA (Xilouris et al., 2018), launched by ESA, started observations in 2017. Two cameras attached to a telescope of 1.2 m in aperture at the National Observatory of Athens observe the flashes at the R- and I-bands almost simultaneously. Derivations of temperatures assuming blackbody radiation are possible. As the first scientific result from the project, Bonanos et al. (2018) obtained temperatures between 1600 and 3100 K for ten flashes. Avdellidou and Vaubaillon (2019) then analyzed 55 flashes in the NELIOTA database. They found the temperature ranging between approximately 1300 and 5800 K with the typical value of about 2500–2600 K. Liakos et al. (2020) summarized results of the first 30 months of the NELIOTA project and showed that the temperatures distribute between 1700 and 5700 K and two-thirds of them were 2000–3500 K. These groups also reported a decrease in temperature with time. The problem of synchronization of the cameras remains though they describe that the synchronization is better than 6 ms (Bonanos et al., 2018; Liakos et al., 2019). For example, one of the flashes (ID 21 in Avdellidou and Vaubaillon 2019, ID28 in Liakos et al., 2020) appears first only in the I-band, then in both bands. The I-band magnitude is almost the same in the successive two frames. The exposure of the R-band camera probably ended before the I-band, then the flash appeared and raised to its peak, and the I-band camera accumulated about half of that total light energy. After the end of the exposure of the I-band camera, the I-band camera accumulated another half of the total light energy in the next frame. The R-band camera accumulated light energy only in the second frame. Typical lunar impact flashes are characterized by sudden brightening and decay, and its time constant is roughly the frame interval of the NELIOTA cameras (33 ms), except for the bright ones such as about 6 in magnitude or brighter. Therefore, even a small difference in exposure timing (e.g., 6 ms) could result in a non-negligible error in the temperature estimation. The scatter of the temperatures in a wide range may be due to the non-perfect synchronization.

The analyses of frames recorded by a color digital camera that was set to a movie mode at 50 frames  $s^{-1}$  also made the temperature estimation possible (Madiedo et al., 2019b). For a bright flash of about 4 in magnitude in visible wavelengths on January 21, 2019, they calculated the B-, V-, and R-magnitude of the flash from the images in the red-, green-, and blue-channel of the image data. Based on the assumption of blackbody radiation and the effective wavelengths of these bands, they obtained 5700 K for the temperature of the flash. There is no problem in the synchronization in this observation. They do not report the temporal evolution of its temperature, probably because of the small aperture (100 mm in diameter) of the telescope to which the camera was attached. At the same time, the flash was recognized for 0.28 s by their other observing system. The temperature is the same as the highest ones obtained by NELIOTA. We will discuss the high temperature later.

Spectral observation of lunar impact flashes, however, has not been conducted yet. As part of the Japan-France collaborative project, that is, the joint observation of meteoroids' impacts as lunar seismic sources (Yamada et al. 2011, 2019), an observation campaign was conducted during the December Geminids activities in 2018. In the campaign, we detected 13 flashes by simple spectral cameras for visible and near-infrared wavelengths (Yanagisawa and Kakinuma, in prep.). Though the resolution of the spectra is quite low, we will examine whether the single blackbody approximation adopted in the multi-band observations is appropriate or not. Further, we will discuss what the dominant source of the lunar impact flashes is.

As one of the major annual meteor showers, the characteristics of Geminids have been well-studied. Their density,  $2.9 \times 10^3 \text{ kg m}^{-3}$ , is the

highest among the meteoroids associated with major showers and the sporadic background (Babadzhanov 2002). Their tensile strength of  $\sim 10^5 \text{ Pa}$  (Beech 2002) suggests that Geminids would not be fluffy aggregates as expected for cometary materials. Spectral observations of meteors show the depletion of sodium in Geminids, probably due to the solar heating during their perihelion passage (Kasuga and Jewitt 2019, Abe et al., 2020). The orbital similarity between Geminids and an asteroid 3200 Phaethon indicates that the meteoroids result from debris shed from the asteroid (reviewed in Vaubaillon et al., 2019). Its perihelion distance is only 0.14 AU, and it is classified as one of the active asteroids (Jewitt et al., 2015). A project of a flyby mission to the asteroid is also in progress for launch in 2022 (Arai et al., 2018). Many lunar impact flashes during the Geminid meteor shower activities have been reported (e.g., Cooke et al., 2007; Yanagisawa et al., 2008; Suggs et al., 2014; Ortiz et al., 2015; Madiedo et al., 2019c; Liakos et al., 2020). The increase of dust around the moon due to the Geminids' lunar impacts was also found by a dust detector onboard the LADEE lunar orbiter in 2013 (Szalay et al., 2018). Spectral observation of Geminid lunar impact flashes would contribute importantly to the studies in these fields.

We describe our observations in Chapter 2 and explain how to derive spectra in Chapter 3. We show the spectra and brightness magnitudes of the lunar impact flashes in Chapter 4. The temperatures of the flashes and meteoroids' masses are also shown in Chapter 4. We discuss the possible problem in a single blackbody model and the source of the flashes in Chapter 5. The conclusions are described in Chapter 6.

## 2. Observations

### 2.1. Observations by spectral cameras

At the University of Electro-Communications (UEC) in Tokyo, Japan ( $35^\circ 39' 28''$  N in latitude,  $139^\circ 32' 37''$  E in longitude, and 80 m in elevation), observations were made with two spectral cameras. One was attached to a Newtonian telescope of an aperture of 450 mm and a focal length of 2025 mm. The other was attached to a Schmidt-Cassegrain telescope with a focal reducer of an aperture of 280 mm and an effective focal length of 940 mm.

The camera attached to the 450 mm telescope is an ASI174MM manufactured by the ZWO company. We removed the cover glass of the camera and glued a blazed type grating on the cover glass of a CMOS image sensor (SONY IMX174MM). The grating has 70 grooves per mm and sold as "Transmission Grating Beamsplitters" by the Edmund Optics company. The other one attached to the 280 mm telescope is a GS3-U3-15S5M-C manufactured by the Point Grey company. We removed the cover glass of the camera and glued the same type of gratings on the cover glass of a CCD image sensor (SONY ICX825). We call the observing system with the 450 mm telescope "System1" and the other "System2" from now on.

We do not apply collimators that make the converging light from the primary mirrors of the telescopes into parallel light rays before the gratings. The converging light directly enters the gratings, passes through them, and is focused on the image planes of the silicon sensor arrays. The no-collimator is not a standard way to use gratings but makes spectral images bright. Spectral resolutions are about 23.9 and 26.5  $\text{nm pixel}^{-1}$  for the System1 and System2, respectively.

For System1, the pixel size of the image sensor is  $5.86 \times 5.86 \mu\text{m}$ , and its resolution,  $1936 \times 1216$  pixels, makes its frame size  $11.3 \times 7.13 \text{ mm}$ . Its field of view is  $19.2 \times 12.1$  arc-minutes when it is attached to the telescope. The gain and exposure time of the camera were set to 40 dB and 16 ms, respectively. Inter-frame durations are negligible, and the frame interval was almost the same as the exposure time, that is, 16 ms. The camera was connected to a personal computer with a USB3.0 cable, and an application, "Fire Capture 2.4," developed by Torsten Edelman, was used for capturing movies in the 16bit-SER format while the bit depth of the camera signal is 12 bits. For the observations of the Flashes A to F described below, movies were stored into a solid-state drive. Then

**Table 1**  
Summary of observations.

Flash	Time (UT) on December 15, 2018	latitude <sup>a</sup>	longitude <sup>a</sup>	Impact angle <sup>b</sup>	number of frames <sup>c</sup>	Observatories <sup>d</sup>
A	08 h 17 m 08s	-21	-39	47	4	1, 2
B	08 h 29 m 35s	30	-57	67	10	1, 2, NU
C	08 h 58 m 50s	30	-40	56	2	1, NU
D	09 h 09 m 48s	-5	-50	66	2	1, NU
E	09 h 44 m 05s	-26	-49	50	2#	2, NU
F	09 h 46 m 16s	5	-70	85	2	1
G	10 h 23 m 07s	-15	-35	48	2	1, NU, Lu
H	10 h 25 m 42s	-60	-71	20	4#	2, NU, Lu
I	10 h 28 m 47s	-12	-48	60	6	1, 2, NU, Lu
J	10 h 35 m 56s	30	-50	63	1	1, NU
K	10 h 54 m 34s	25	-55	70	2	1, NU
L	11 h 22 m 13s	-3	-74	76	4	1, 2, NU, Lu
M	11 h 35 m 52s	23	-29	50	1	1, 2, NU

<sup>a</sup> Selenographic latitude and east longitude.

<sup>b</sup> Measured from local horizons.

<sup>c</sup> The number of frames, where each flash is recognized, observed by System1. Those observed by System2 are shown with #.

<sup>d</sup> Systems or observatories that detected each flash. 1: System1, 2: System2, NU: Nihon Univ, and Lu: Lulin observatory.

the pixels were binned into  $2 \times 2$ , and movies were stored into a hard disk drive for the other flashes. The binning makes the spectral resolution about  $47.8 \text{ nm pixel}^{-1}$ .

For Sytem2, the pixel size of the image sensor is  $6.45 \times 6.45 \mu\text{m}$ , and its resolution,  $1384 \times 1032$  pixels, makes its frame size  $8.93 \times 6.66 \text{ mm}$ . Its field of view is  $32.7 \times 24.2$  arc-minutes when it is attached to the telescope. The gain and exposure time of the camera were set to 24 dB and 25 ms, respectively. The frame interval was 25 ms. The camera was connected to a personal computer with a USB3.0 cable, and "Fire Capture 2.5" captured movies into a hard disk drive in the 16bit-SER format while the bit depth of the camera signal is 14 bits. No binning was applied.

An observation campaign expecting lunar impact flashes due to Geminids was conducted between 10th and December 16, 2018. The weather was fine at UEC only in the night on the 15th. The age of the moon was 8.0–8.2 (a waxing moon). System1 and System2 were operated for 08:04:08–13:08:56 UT and for 07:58:10–13:11:38 UT, respectively. After the observations, an application, "ser\_scan" developed by us, scanned the SER movies and found 13 flash candidates in the movies recorded by System1 and System2. We named them A to M flashes (Table 1). Supplementary video (online version only) shows the movie of Flash I. Madiedo et al., 2019c observed at least 11 lunar impact flashes on 13th and December 14, 2018 from two different sites in Spain. They calculated the probability of these flashes being associated with Geminids to be 90%. The flashes we observed on 15th December, therefore, must be generated due to the impacts of the Geminids' meteoroids onto the lunar surface.

Fire Capture stamps the time of a computer clock on each frame in a movie. The intervals of the stamped times should be constant and the same as the exposure time if the stamped times are exact and there is no frame drop. The frame drops occur when image data transferred through the USB3.0 cable and stored into the disk exceeds the capability of the systems. We examined the intervals of the stamped times in successive frames over plus-minus 1 min around the times of the flashes. They fluctuate around 16 ms for System1, and 25 ms for System2. However, a longer interval is followed by a shorter one. Therefore, the average of the intervals over some frames is constant. We decided that the recording speed into the drive is fast enough and there is no frame drop. The application seems to stamp time when it stores a frame in a drive. It is slightly different from the time of the start or the end of the exposure of the camera. The difference would lead to the fluctuation of the intervals of stamped times.

## 2.2. Observations at the other observatories

Observations with normal digital movie cameras were conducted at Nihon University (NU) in Chiba-prefecture, Japan ( $35^{\circ}43'31''$  N in latitude,  $140^{\circ}03'32''$  E in longitude, and 28 m in elevation) by a telescope of

400 mm in aperture. At Lulin Astronomical Observatory, Taiwan ( $23^{\circ}28'07''$  N in latitude,  $120^{\circ}52'25''$  E in longitude, and 2862 m in elevation), they observed by two telescopes of 152 mm and 200 mm in apertures and normal digital movie cameras.

All the flashes, except A and F, were detected simultaneously at NU, which was located 47 km east of UEC. They did not start observations at the time of Flash A. Flash F was out of the field of view of their camera. Lulin observatory, which was located 2300 km south-west of UEC along the earth's surface, started observations later at 10:16 UT due to the local time difference between Japan and Taiwan. Flashes G to M were expected to be found, and we confirmed four of them (Flashes G, H, I, and L). They paused observations at the times of Flashes J and M. Flash K was not detected probably due to the frame drop described in the previous section.

The most significant source of the false-positive detections of lunar impact flashes is the reflection of sunlight by artificial satellites or space debris. The best way to distinguish the lunar flashes from the satellite glints is by examining the movies obtained at least two observatories separated far enough. Most of the human-made objects are orbiting in and below the geosynchronous orbit. The distance to them from observatories is at most about 40,000 km, while the moon is about ten times far away. Their positions on the lunar disk are therefore different between the observatories, while a lunar flash appears at the same position. Simultaneous detections of the G, H, I, and L flashes both in Japan and Taiwan clearly show that they were the lunar phenomena. For the other flashes, we calculated the parallax of a satellite located at 40,000 km in the lunar direction between the observations at UEC and NU. It is about one-tenth of the angular diameter of the moon. We examined the positions of the flash-images on the lunar disk on the frames obtained by the two observatories. They agree with the accuracy of one-hundredth of the lunar angular diameter despite the blurred images due to the spectral dispersion of images obtained by the spectral cameras. The possibility of satellite glints thus is discarded completely for the eleven flashes. For the other two flashes, we examined whether cataloged satellites or space debris passed in front of the lunar disk accidentally. We examined the positions of 17,754 satellites or space debris listed in the two-line element orbital datasets downloaded from Space-Track<sup>1</sup> on both 15th and December 17, 2018 using an application "StellaNavigator 10" by the Astro Arts company. We found no human-made object around the moon that moved slowly enough to be misinterpreted as a lunar flash at the times of Flash A. A geostationary satellite, Gorizont 23, was found at  $0.5^{\circ}$  from the lunar disk center in the celestial south-east direction at the time of Flash F. It was close to the south-eastern edge of the disk 1 min before

<sup>1</sup> Space-track: <https://www.space-track.org/>, last access on 4th March. 2020.

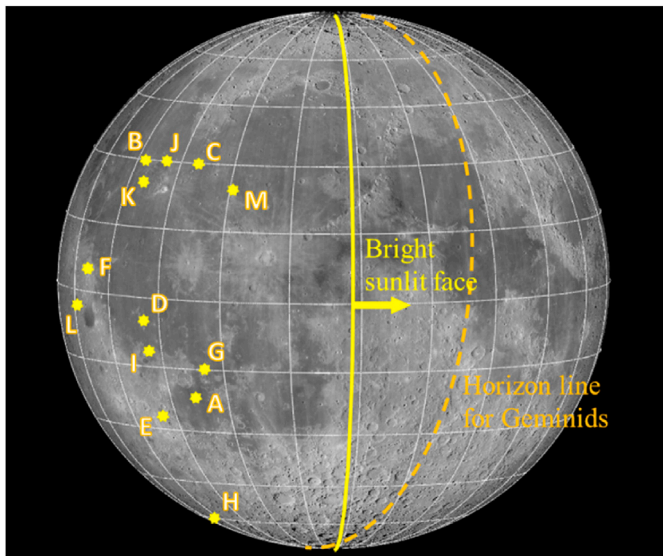


**Fig. 1.** Locations of the lunar impact flashes observed on 15th December, 2018. Geminids could hit the lunar surface to the left side of the orange broken line. The sunlight illuminated the right side of the solid yellow line. The lunar image was obtained by using the Virtual Moon Atlas<sup>2</sup>. (For interpretation of the references to color in this figure legend, the reader is referred to the Web version of this article.)

of the flash. We do not know the accuracy of the orbital data and the calculations in the application; however, the sudden brightening and an afterglow of this event support it to be a lunar impact flash.

The selenographic latitudes and longitudes of the flashes (Table 1 and Fig. 1) were determined on the images recorded at NU. For the flashes that were not recorded there, the locations were determined on the images by System1 or System2. Despite no sunlight illumination, we can recognize the bright Aristarchus region and the dark Grimaldi crater on the night side images of the moon illuminated by the earth (earthshine). Based on the positions of the flashes relative to them, we determined the latitudes and longitudes on the maps generated by an application “Virtual Moon Atlas”<sup>2</sup>. The impact angles measured from local lunar horizons in the table were calculated assuming the Geminids impacts, the radiant of which is 112° and 33°, respectively in right ascension and declination.

The flashes appear brightest in the 1st frames of frame sequences where they are recognized. The times at the 1st frames are listed in Table 1. The computer clock at NU was adjusted through an internet signal, while those at UEC were adjusted manually. The stamped times of System1 and System2 were therefore corrected to agree to those at NU, and shown in the table.

### 3. Spectral analyses

The spectral flux densities  $\bar{F}_{flash}(\lambda)$  at wavelength  $\lambda$  of a flash is calculated as

$$\bar{F}_{flash}(\lambda) = N_{flash}(\lambda) / N_{star}(\lambda) \cdot k \cdot \pi B_{T_{star}}(\lambda) \quad (1)$$

where  $N_{flash}(\lambda)$  and  $N_{star}(\lambda)$  are count numbers as shown in Fig. 2b after the corrections described below. Their subscripts represent a flash and a comparison star.  $B_{T_{star}}(\lambda)$  represents the Planck function at temperature  $T_{star}$ , and  $k$  is a non-dimensional value related to the brightness of the star.  $T_{star}$  is the effective temperature of the star derived from its color

<sup>2</sup> Virtual moon Atlas: <https://www.ap-i.net/avl/en/start/>, last access on 4th March, 2020.

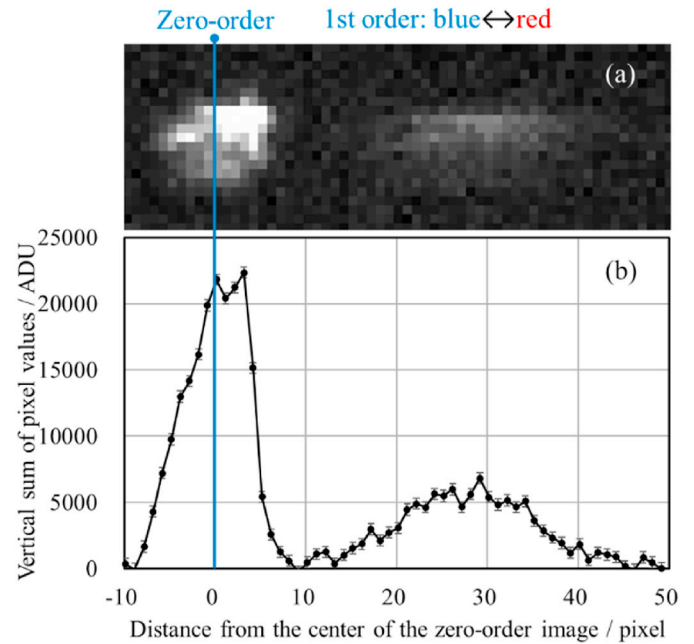


**Fig. 2.** The spectral image (a) and its count profile (b). The pixel values along each vertical column are added and plotted in the count profile. We convert the distance from the center of brightness of the zero-order image to a wavelength, after some corrections described in the text. The image (a) is a portion of the 1st frame of Flash B after the background subtraction (flipped horizontally).

index,  $B - V$ , and Table 3 in Flower (1996), where  $B$  and  $V$  denote respectively the B- and V-magnitudes. We obtained  $B$  and  $V$  from the SIMBAD<sup>3</sup> database. It should be noted that  $\bar{F}_{flash}(\lambda)$  is a temporal average of the flux  $F_{flash}(\lambda, t)$  over an exposure time of the cameras  $\Delta t$  as

$$\bar{F}_{flash}(\lambda) = \frac{1}{\Delta t} \int_t^{t+\Delta t} F_{flash}(\lambda, t) \cdot dt \quad (2)$$

Therefore, when the duration of the peak at the beginning of a flash is shorter than the exposure time,  $\bar{F}_{flash}(\lambda)$  underestimates its real flux. We applied the following corrections to  $N_{flash}(\lambda)$  and  $N_{star}(\lambda)$  before using Eq. (1).

#### 3.1. Dark frame correction

For every observation of flashes and stars, we recorded a hundred frames of dark field (no light input) with the same gains and exposure times just before or just after the observations. We averaged a hundred frames and obtained the dark frame for each observation. We subtracted the dark frame from each frame in raw SER movie files before any other processing.

#### 3.2. Background subtraction and counting of pixel values

We averaged about two hundred frames before and after a flash. The averaged image was subtracted from a frame where the flash was recognized. We thus obtained a background-subtracted-image (Fig. 2a). In the averaging process, we also calculated the temporal standard deviation of count values for each pixel. The average of the standard deviations in a counting area of the background-subtracted-image was used to calculate the error bars in Fig. 2b.

In both System1 and System2, the spectral dispersion direction is

<sup>3</sup> SIMBAD: <http://simbad.u-strasbg.fr/simbad/>, last access on 4th March, 2020.

horizontal in images. We summed pixel values of the background-subtracted-image over some pixels along a column. The vertical range of the columns is determined visually. We thus obtained the summed count as a function of horizontal position (Fig. 2b).

In the analyses of movie frames of a star, we averaged about a hundred frames. Then, we summed pixel values of the averaged image over some pixels along each column. We obtained a background count for each column using pixel values in the upper and lower portion of the column, where the pixel values were not affected by the star. After the correction of the background, the summed counts as is shown in Fig. 2b are obtained.

### 3.3. Corrections for the atmospheric dispersion

Light rays from a star bend due to the atmospheric refraction, and the star appears higher above the horizon than it actually is. Wavelength dependence of the refraction angle makes blue image up and red image down relatively and leads to a vertically elongated image of the star. If it were not for the atmosphere, spectral dispersion by the grating would make a zero-order point image of a star and a 1st order line image (spectral image). The wavelength dependence distorts both the zero-order and the 1st order images. If the dispersion direction by the grating is parallel to the local horizon, blue components of a stellar image shift up and red components shift down due to the atmospheric dispersion. Then, the zero-order image slightly elongates vertically, and the spectral image bends a little. The dependence is well formulated as a function of wavelength and zenith angle (Schubert and Walterscheid 1999). We considered the atmospheric dispersion and converted the x-coordinate in Fig. 2b to wavelengths for each of the flashes and comparison stars (see Yanagisawa and Kakinuma, in prep. for details).

### 3.4. Corrections for the 2nd order image

In the images of flashes and stars observed by our spectral cameras, the 1st order image of, for example, 800 nm, is contaminated by the 2nd order image of 400 nm. We must, therefore, remove the contribution from the 2nd order image. We measured the ratios of the brightness intensities between the 2nd and the 1st order images of a monochromatic artificial star in laboratory experiments for wavelengths between 400 nm and 800 nm. The relationship between the ratio and wavelengths was expressed by a polynomial function of wavelengths and used for subtracting the counts of the 2nd order images from the 1st order counts. The function is obtained independently for System1 and System2. In the laboratory experiments with the spectral camera in System2, we substituted a commercial camera lens for the 280 mm telescope. The substitution may lead to some errors in the coefficients of the polynomial function.

### 3.5. Comparison stars

We approximated that the spectrum of a comparison star was expressed by the Planck function at its effective temperature multiplied by some value related to its brightness, that is,  $k \cdot \pi B_{T\_star}(\lambda)$  in Eq. (1). The value  $k$  was calculated from its V-magnitude. The spectral flux density of a flash is then derived from the temperature, the magnitude, and the count ratios between the flash and the star, according to Eq. (1). We used Pollux ( $\beta$  Gem) observed on March 26, 2019 as the comparison star for System1 because the stars observed on the night of the Geminids flashes were faint or M in spectral type whose spectra were not approximated well by the Planck function. The weather was fine on both nights despite the three months difference in time. We derived the spectrum of a faint G type main-sequence star, HD222799, observed on the night of the Geminids flashes according to the procedures described in this Chapter (Supplementary Fig. S in the online version), where the comparison star was Pollux. The spectrum is well approximated by a blackbody spectrum of 5400 K, and its V-magnitude, calculated by Eq. (3) in Section 4.2, is

8.4. On the other hand, the B- and V-magnitudes of the star in SIMBAD<sup>3</sup> are respectively 9.59 and 8.82. Its effective temperature is 5359 K, according to  $B - V = 0.77$  and Table 3 in Flower (1996). Despite the 0.4 difference in V-magnitude, the agreement of the temperatures validates the use of Pollux as the comparison star for studying the spectral features of the impact flashes. For System2, we used HD222465 observed on the night of Geminids flashes. This star is an F6 type main-sequence star of 7.2 in V-magnitude (SIMBAD<sup>3</sup>). The spectrum of HD222799 mentioned above observed on the same night by System2, obtained with the comparison star HD222465, shows 5600 K and 8.9 in V-magnitude. Both values approximately agree to the temperature and the magnitude based on SIMBAD<sup>3</sup> and Flower (1996). The agreement validates the use of HD222465 as a comparison star for System2.

### 3.6. Corrections for the atmospheric absorption

A flash and a comparison star are not necessarily recorded in the same movie frames. They are usually observed independently at different times and in different directions. We made corrections for the atmospheric absorption with the assumption that there was no difference in atmospheric conditions, such as water vapor and aerosol contents, among observations. The atmospheric transmittance depends on zenith angles as well as wavelengths. We obtained the zenithal atmospheric transmittance as a function of wavelengths between 400 nm and 1000 nm with the following three parameters using a free web application of MODTRAN<sup>4</sup>; summer, mid-latitude, and urban. The temperature in Tokyo, Japan in between December and March is not so cold as typical mid-latitude countries. We adopted “summer” therefore instead of “winter” as a parameter. The transmittance between 300 nm and 400 nm was obtained from Table 11.25 in Schubert and Walterscheid (1999).

### 3.7. Spectral flat-field correction

One of the drawbacks of our spectral cameras is that the count profiles as shown in Fig. 2b depends on where the spectral image (Fig. 2a) appears in a frame (Yanagisawa and Kakinuma, in prep.). For example, the profiles derived from images observed in the left-side area in frames are different from those in the right-side area. To avoid the problem, we recorded the comparison star Pollux along twenty horizontal lines in movie frames by System1. The frames where the star is located nearest to the flash coordinate on a frame were used to obtain the count profile of the comparison star.

On the other hand, a star, HD166, was observed on November 15, 2018 at 25 points distributed uniformly in the field of view of System2. We compared a profile obtained from a movie where HD166 appeared nearest to the flash coordinate with the other profile obtained from a movie where HD166 appeared nearest to the comparison star (HD222465). The results of the comparisons were used in the spectral flat-field corrections. HD166 is a variable star, so we did not use it as a comparison star as we did for System1.

The correction is almost complete in System1 but not in System2. The correction for the 2nd order image described in Section 3.4 is also more accurate for System1 than for System2. Furthermore, the aperture of the telescope is larger, and the framing rate of the camera is higher for System1 than for System2. Therefore, in the following chapter, we show the results obtained by System1 unless the observations were interrupted in the system.

## 4. Results

### 4.1. Spectra

The spectral flux densities  $\bar{F}_{flash}(\lambda)$ , observed outside the terrestrial atmosphere, of bright flashes are shown in Figs. 3–7. These spectra are

<sup>4</sup> MODTRAN: <http://modtran.spectral.com/>, last access on 4th Mar. 2020.

reliable between 400 nm and 870 nm in wavelengths except Flash H (Fig. 5), which was observed by System2. Spectra of the other flashes are shown in the Supplementary figures (online version only). The analyses of the subsequent frames are possible for these bright flashes, and we also show their spectra. Flash A is also bright, but a probable mechanical twitch of the telescope in System1 blurred an image in the 1st frame where the flash abruptly appeared. Therefore, the reliable spectrum was not obtained for the frame. The twitch would also have occurred in System1 at Flash M, and the blurred image prohibited the derivation of the reliable spectrum.

Error bars in the figures are based on the temporal variation of the background described in Section 3.2. They include photon shot noise and electric noises. The same kinds of noise for the comparison stars are not considered because the averages of about a hundred frames reduce the noises. The effect of the atmospheric scintillation discussed later is not included in the error bars. Error bars are not shown for the 2nd and the 3rd frames, but they are almost the same as for the 1st frame at the same wavelength.

Spectral flux densities in the wavelength range between 300 nm and 400 nm might be overestimated because of the following reasons. There could be some non-negligible absorptions in the stellar atmosphere in this range. The blackbody approximations for the comparison stars, Pollux and HD222465, could then overestimate the real flux. That is to say,  $k \cdot \pi B_{T\_star}(\lambda)$  in Eq. (1) could overestimate the real flux from the stars, then  $F_{flash}(\lambda)$  could also be overestimated. Besides, terrestrial atmospheric absorptions are 55% at 400 nm and 100% at 300 nm in the zenithal direction (Schubert and Walterscheid 1999) and more significant in the non-zenithal directions. The absorption in this wavelength range is more variable than in the longer wavelengths. It may have been deeper on the nights of the comparison stars' observations in Japanese spring and autumn than on the night of the Geminids flashes in winter.  $N_{star}(\lambda)$  in Eq. (1) could be larger if we had observed the stars on 15th December. These two possibilities could cause the overestimations at these wavelengths.

The uncertainties, which are related to the correction for the 2nd order image and not included in the error bars in the figures, should be considered at long wavelengths. Corrections are relatively small for the

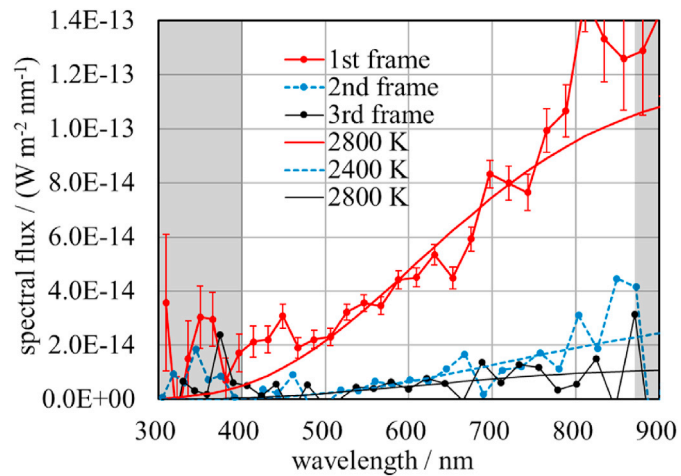


Fig. 3. Spectra of Flash B, observed outside the terrestrial atmosphere, at the 1st (red solid polygonal line), the 2nd (blue broken polygonal line), and the 3rd (black thin polygonal line) frames observed by System1. Error bars represent one standard deviation of the background fluctuation. We do not show error bars for the 2nd and the 3rd frames, but they are almost the same as for the 1st frame at the same wavelength. The fluxes are reliable between 400 nm and 870 nm in wavelengths (the non-shaded area). Blackbody spectra were best-fitted to the plots in the non-shaded area and are shown by smooth curves. We show the blackbody temperatures in the plot area. Both the exposure time and the frame interval of the camera were 16 ms. (For interpretation of the references to color in this figure legend, the reader is referred to the Web version of this article.)

flashes but not negligible for the comparison stars because the stars are bluer than the recorded flashes (dominated by latter stages of the process) and the contribution of a 400 nm light to an 800 nm image is for

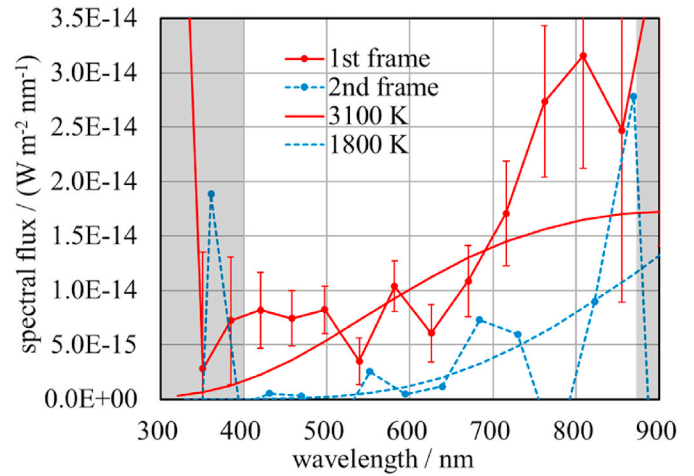


Fig. 4. Spectra of Flash G observed by System1.

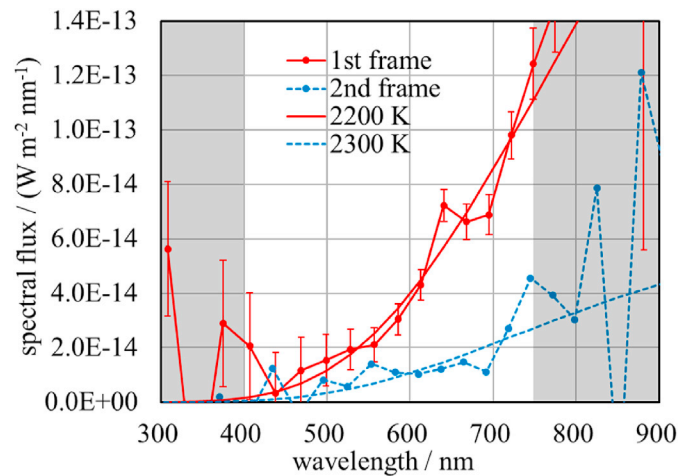


Fig. 5. Spectra of Flash H observed by System2. The observation was interrupted in System1. Both the exposure time and the frame interval are 25 ms.

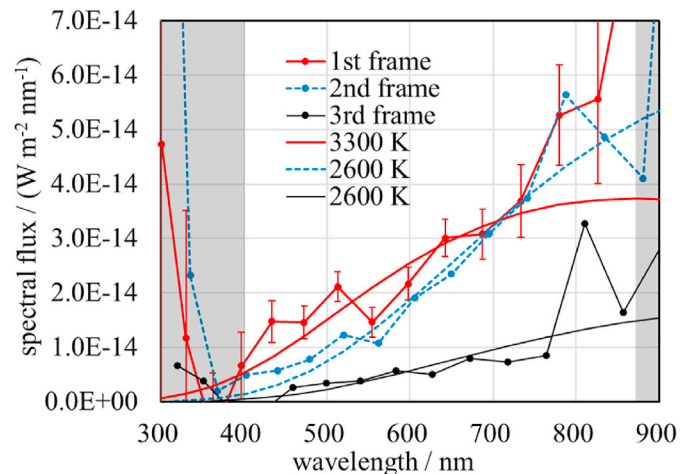


Fig. 6. Spectra of Flash I observed by System1.

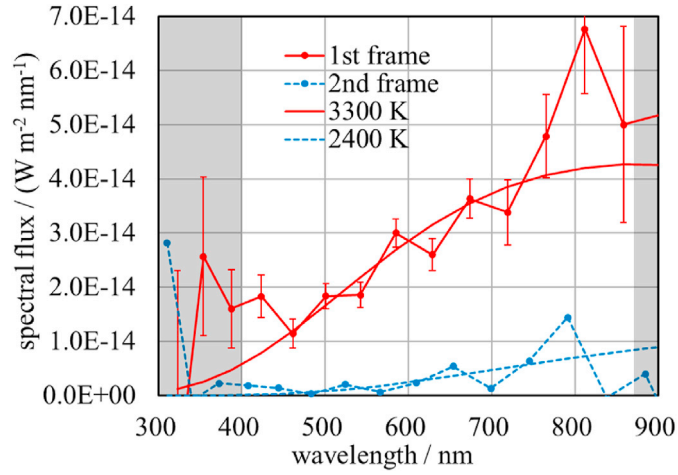


Fig. 7. Spectra of Flash L observed by System1.

example more significant for the stars. For the comparison star, Pollux, observed by System1, the contribution of  $\lambda/2$  light exceeds 10% at about  $\lambda = 870$  nm. The contribution exceeds 10% at about  $\lambda = 750$  nm in the case of System2. The coefficients of the polynomials used for the correction of the 2nd order light could be associated with non-negligible errors, especially for System2. The errors in  $N_{star}(\lambda)$  lead to the errors in  $\bar{F}_{flash}(\lambda)$  plotted in Figs. 3–7.

To examine the temporal variation of spectral features due to atmospheric scintillations, we obtained count profiles as Fig. 2b for each of the frames of a bright star, HD4128 ( $\beta$  Cet), observed at  $54^\circ$  in zenith angle on November 9, 2017 by System1. The count profile fluctuates with time with the amplitude (standard deviation) of about 15%. Though the scintillation varies day by day, we expect it would not make the spectra unreliable. However, detailed discussions on a single spectrum could lead to incorrect conclusions. We should discuss with a broad view of all the spectra. We did not examine the temporal variation in the same way by using System2. The observed spectra may be affected more significantly by the atmospheric scintillations in System2 than System1 because of the smaller aperture of the telescope.

The amplitudes of the spectral flux densities and brightness magnitudes for the 1st frame described in the next section importantly depend on the time lag between the beginnings of a flash and a camera exposure, as illustrated in Fig. 8. The lightcurve of a typical lunar impact flash is characterized by a sudden brightening and a decrease in brightness with a time constant of about a few of the exposure time of the movie camera (e.g., Yanagisawa and Kisaichi 2002). When the exposure starts around the beginning of a flash, its image in the 1st frame appears bright. On the other hand, when the exposure starts earlier, the flash appears less bright. As Eq. (2) shows, the spectral flux densities  $\bar{F}_{flash}(\lambda)$  in Figs. 3–7 show averages over the camera exposure, and their amplitude at the 1st frame depends on the time lag, which we do not know. Longer exposure duration of System2 could statistically lead to lower flux densities and darker magnitudes for the 1st frames than those derived from System1 observations. The blackbody temperatures described below would also depend on the time lag and the exposure time to some extent if the temperature changes quickly.

A blackbody spectrum was best-fitted to each spectrum. It is drawn as a smooth line, and we show the blackbody temperature in each figure. The plots in the reliable wavelength ranges were used in the best-fittings. We tried to fit Planck functions of different temperatures to the observed spectra and estimated the error in the temperatures to be about 300 K. We show the temporal variations of the temperatures in Fig. 9. The temperatures and their decreases with time roughly agree to the previous results (Avdellidou and Vaubaillon 2019; Liakos et al., 2020).

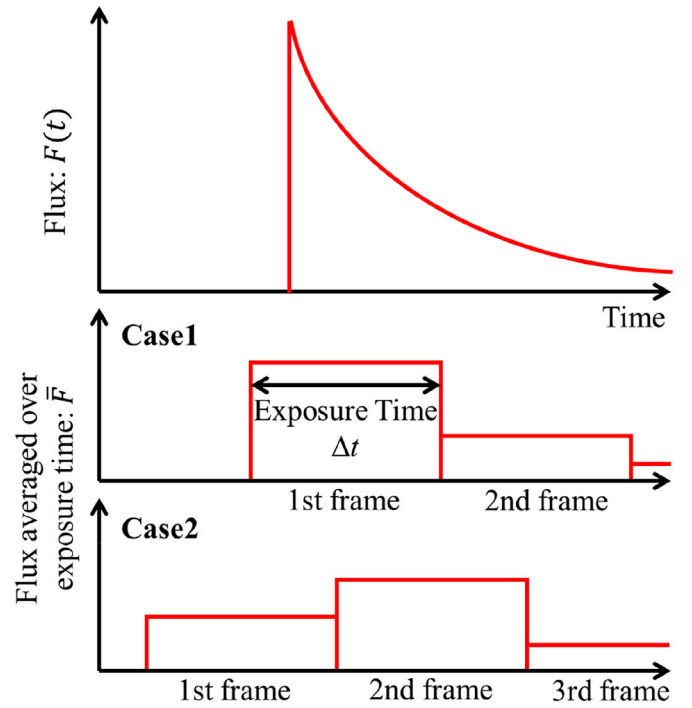


Fig. 8. Effect of the time lag between the beginnings of a flash and exposure of a camera on observed fluxes. The exposure of the 1st frame started just before the beginning of the flash in Case1; then, the averaged flux is relatively large. The exposure started much before the beginning of the flash in Case2; then, the averaged flux is relatively small.

#### 4.2. Magnitudes and meteoroid masses

The magnitudes  $m_{flash}$  were calculated according to the following formula for the V-, R-, and I-bands independently;

$$m_{flash} - m_{sun} = -2.5 \log_{10} \left[ \frac{\int \bar{F}_{flash}(\lambda) R(\lambda) d\lambda}{\int F_{sun}(\lambda) R(\lambda) d\lambda} \right] \quad (3)$$

where  $m_{sun}$  is the solar magnitude and  $R(\lambda)$  is the response function for a band (Bessell 2005). The integrals were calculated numerically, where we used the plot intervals in the spectral figures as  $d\lambda$ . We truncated the integration at 870 nm and 750 nm for the flashes observed by System1 and System2 respectively, while there was no truncation for the sun. For the System2, this makes the R-magnitude a little dimmer and prohibits the derivation of the I-magnitude because its effective wavelength is 800 nm (Bessell 2005). The magnitudes at the 1st frames are listed in Table 2. It should be noted that there are uncertainties in these magnitudes due to an unknown parameter, the time lag.

Luminous energy  $\mathcal{E}_{flash}$ , observed outside the terrestrial atmosphere, were calculated as

$$\mathcal{E}_{flash} = \sum \left[ \int \bar{F}_{flash}(\lambda) R_{video}(\lambda) d\lambda \right] \Delta t \quad (4)$$

where  $R_{video}(\lambda)$  is the response function of the video camera, WAT-100 N, manufactured by WATEC company. We call this “video-band” from now on.  $R_{video}(\lambda)$  is non-zero between 310 nm and 1000 nm in wavelength and has a peak value of 1.0 at 615 nm. The integrals were calculated numerically over the reliable wavelength ranges. We used the plot intervals in the spectral figures as  $d\lambda$ .  $\Delta t$  is the exposure time for each frame and the summation in Eq. (4) is calculated over the frames for which we obtained spectra.

The luminous energy at the moon was obtained as

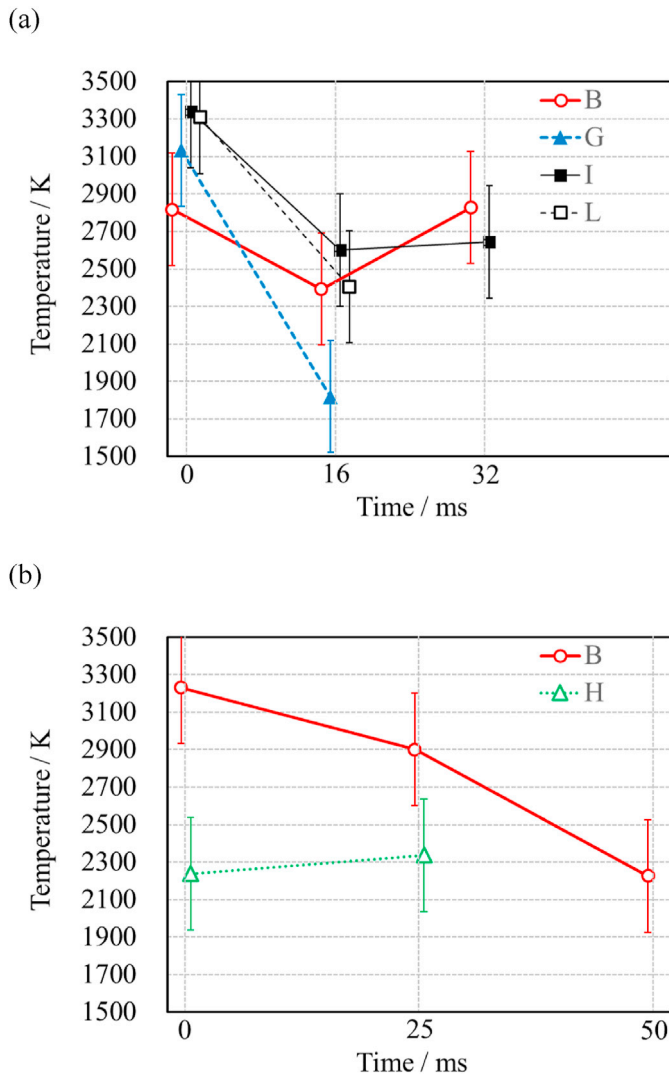


**Fig. 9.** Temporal variations of the blackbody temperatures of the bright flashes observed by System1 (a) and System2 (b). The temperature for a frame in which a flash appears first is plotted at zero in the horizontal axis. That for the 2nd frame is plotted at 16 ms and 25 ms (frame intervals) for System1 and System2, respectively. The abscissa does not necessarily represent the time after the beginning of a flash. There is an uncertainty of 16 ms or 25 ms. The error of the temperatures is estimated to be about 300 K.

$$E_{flash} = \mathcal{E}_{flash} \cdot 4\pi r^2 \quad (5)$$

where  $r$  is the distance between the moon and the observatory ( $4.0 \times 10^5$  km), and we assume the flashes were radiated uniformly into  $4\pi$  steradians.

The impact energy, that is, the kinetic energy of the meteoroid is obtained as

$$E_{imp} = \eta E_{flash} \quad (6)$$

where  $\eta$  is the luminous efficiency. Some studies (Bellot Rubio et al. 2000a, 2000b; Moser et al., 2010) show its value to be between 0.1% and 0.2%. We adopted 0.2% in our calculations. The meteoroids that hit the lunar surface must be Geminids; therefore, we calculated their masses in Table 2 with their impact velocity of  $35 \text{ km s}^{-1}$ . There is no problem with the time lag because of the multiplication by  $\Delta t$  and the summation in Eq. (4). The real masses would be a little bit larger than the ones listed in the table due to the truncations of the integration range in Eq. (4).

**Table 2**

Summary of the magnitudes of the flashes at the 1st frames of their movie sequences.

Flash	magnitude by System1			magnitude by System2		mass/g
	V	R	I	V	R	
A				8.7	7.7	130 <sup>a</sup>
B	7.5	6.2	5.1	8.4	7.4	600
C	11.4	8.7	7.6			35
D	9.4	8.5	8.8			48
E				9.8	9.6	- <sup>b</sup>
F	10.6	9.9	- <sup>b</sup>			11
G	9.3	7.9	6.6			130
H				7.9	6.2	660 <sup>a</sup>
I	8.1	7.0	6.1	8.9	7.6	490
J	10.0	9.0	- <sup>b</sup>			26
K	9.4	8.3	6.9			82
L	8.0	6.8	5.8	8.5	7.3	290
M				8.8	9.1	100 <sup>a</sup>

<sup>a</sup> The meteoroid masses were derived from the observations by System2. The masses for the others were derived from the observations by System1.

<sup>b</sup> Integrals of fluxes over the I-band or the video-band wavelengths are negative.

## 5. Discussion

Before discussing the spectra of the lunar impact flashes, we examine the brightness magnitudes at the 1st frames in Table 2. The magnitudes were obtained by both System1 and System2 for the Flashes B, I, and L (Table 2). Those by System2 is larger (dimmer) by about 0.7 on average than those by System1 for both V- and R-magnitude. The most probable cause of this disagreement could be the difference in the exposure time between System1 (16 ms) and System2 (25 ms). If the duration of the bright phase at the beginning of a flash is much shorter than the exposure time,  $N_{flash}(\lambda)$  in Eq. (1) does not depend importantly on the exposure time, while  $N_{star}(\lambda)$  increases linearly with the exposure time. With the increase of the exposure time, the spectral flux density  $\bar{F}_{flash}(\lambda)$  reduces, and the magnitude increases. The difference in the exposure time, 16 ms vs. 25 ms, leads to a difference of 0.5 in magnitude in this case. Because of the dependence of the magnitudes on the exposure time, we must be careful when we compare the magnitude distribution between, for example, Suggs et al. (2014) and Liakos et al. (2020), where their exposure times are 16 ms and 23 ms respectively.

The spectra of the bright flashes shown in Figs. 3–7 are continuous and increase almost monotonically with wavelengths. Those of the other flashes are much noisier but show the same tendency. Despite the uncertainty of the magnitudes discussed above, the color indices that are the differences in the magnitudes between the two wavelength bands do not depend on the exposure time at all. The average and the standard deviation of the color index,  $V - R$ , calculated from the magnitudes listed in Table 2 for both System1 and System2 are  $1.1 \pm 0.6$ , and those of  $R - I$  are  $0.9 \pm 0.6$ . Besides, the average and the standard deviation of  $R - I$  calculated for the 1st frame in Table 1 in Bonanos et al. (2018) is  $1.2 \pm 0.4$  and almost agrees to our result. Our smaller value in  $R - I$  may be due to the truncation of the integration at 870 nm in calculating the I-magnitudes by Eq. (3). The truncation makes the I-magnitude a little bit larger (dimmer), then makes  $R - I$  smaller. It is interesting to note that the impact flashes by Geminids and other ones observed by Bonanos et al. (2018) show similar  $R - I$  on average. Both  $V - R$  and  $R - I$  of the sun are 0.35 (Ramírez et al., 2012) and smaller than the indices of the flashes. One can say that lunar impact flashes are redder than the sun in the visible and near-infrared wavelengths, though they may appear bluer at the very beginnings if we observe them with higher time resolution.

As a first approximation, the blackbody spectra of single temperatures fit the observed spectra of the lunar impact flashes in the visible and near-infrared wavelengths (Figs. 3–7). However, the fittings for the 1st frames seem to be less satisfactory than for the 2nd and the 3rd frames. There may be excess fluxes in the short wavelengths less than around 600 nm

for the 1st frames. This is not unnatural because each part of a plume or ejecta must radiate at different temperatures at a time, and the radiation from some part could not necessarily dominate the total radiation. Furthermore, the temperature distribution in the plume or ejecta must vary with time during an exposure time for a movie frame, e.g., 16 ms. The nonuniformity and the time variation have been observed in laboratory experiments in the initial stages (within several tens of microseconds) of impact phenomena (Schultz and Eberhardy 2015). As the second approximation, we fitted the composite of two blackbody spectra to the plots in each of the 1st frame spectra (Fig. 10). We made the fittings visually while changing the two temperatures and the two intensities of the blackbody radiations variously. The composites seem to approximate each of the observed spectra much better than the single blackbody spectra. The composites consist of blackbody radiations, one at about 6000 K and the other at about 2000 K.

The former temperature is close to the maximums observed in laboratory impact experiments. Sugita et al. (1998) and Sugita and Schultz (1999) observed the spectra for the first few microseconds of the flashes at collisions of spherical quartz and copper projectiles of less than 1 cm in diameter with dolomite blocks at about 5 km s<sup>-1</sup>. They analyzed the ratios among line emission intensities of Ca and Cu and derived the excitation temperatures around 6000 K. They supposed that they observed jets that squirted out from the interface between the projectiles and targets (e.g., Section 4.4 in Melosh 1989).

After the jetting, still in the initial stage of impact phenomena, self-luminous plumes, which consist of gas and dust, and are sometimes

called “vapor plume” or “vapor cloud,” are observed in laboratory experiments (Section 5.3 in Melosh 1989, Fig. 19 in Schultz et al., 2007). They are observed for more than several tens of microseconds. The time-integrated light energy would be larger for the plumes than the jets. Furthermore, thin layers of carbon, which would be contained in meteoroids, over dolomite powder targets increase the continuum radiation from the plumes (Schultz et al., 2007; Schultz and Eberhardy 2015). The plumes could be bright enough to appear as the high-temperature components.

Ernst and Schultz (2004) conducted experiments with pumice dust targets and subcentimeter Pyrex projectiles at about 5 km s<sup>-1</sup>. The blackbody temperatures of the plumes were measured by multi-band photometry. They are about 4000 K for the first 20 μs. Similar experiments with 20 mm thick dolomite plates and polycarbonate projectiles at less than 4.2 km s<sup>-1</sup> also show about 4000 K (Tang et al., 2015). These temperatures are lower than 6000 K of the high-temperature components. However, the plume temperature could increase with impact velocities as suggested by Ernst and Schultz (2002). Consequently, the expanding, self-luminous vapor plume would be the major contributor to the high-temperature component captured in the lunar impact flash.

We expected the low-temperature components to show the temperatures at the 2nd and the 3rd frames, but 2000 K is a little bit too low. The disagreement may be due to the oversimplification of the two-component model. Despite the possibility of oversimplification, the better fits of the model indicate that the single blackbody model adopted in Figs. 3–7 and previous works (e.g., Avdellidou and Vaubaillon 2019; Liakos et al.,

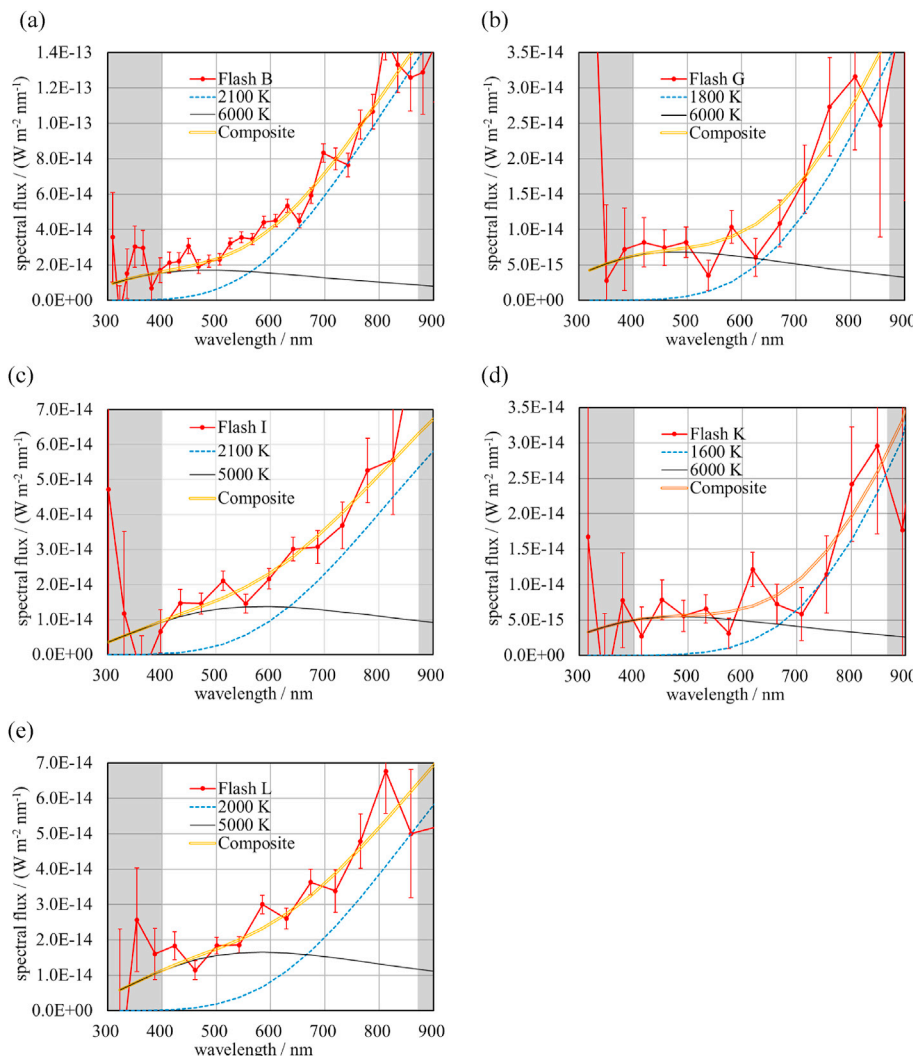


Fig. 10. Spectra at the 1st frames of bright flashes (red solid polygonal lines) except Flash H. These were observed by System1 with 16 ms in the exposure time of the camera. Error bars represent one standard deviation of the background fluctuation. The fluxes are reliable between 400 nm and 870 nm in wavelengths (the non-shaded area). A composite of two blackbody spectra (blue broken and black thin smooth lines) was fitted visually to the plots in each of the spectra and is shown by a smooth double curve. (For interpretation of the references to color in this figure legend, the reader is referred to the Web version of this article.)

2020) may not be appropriate to derive the physically meaningful temperatures for the 1st frames (at the beginning of flashes). It may be better to refer to the 1st frame temperatures as “apparent temperatures.”

The apparent temperatures at the 1st frames obtained assuming a single blackbody would depend on the wavelength range used to derive them. The high- and low-temperature components respectively dominate visible and near-infrared wavelengths in the spectra (Fig. 10). Therefore, the temperatures derived from visible wavelengths would tend to be higher than temperatures mainly from near-infrared wavelengths. Temperatures at the 1st frames obtained in the NELIOTA project by Bonanos et al. (2018), Avdellidou and Vaubaillon (2019), and Liakos et al. (2020) from the brightness ratios between the R- and I-bands (red and near-infrared wavelengths) distribute over 1300–5800 K. Whereas, Madiedo et al. (2019b) obtained almost the upper end of this distribution, 5700 K, for a bright flash from the ratios among B-, V-, and R-bands (visible wavelengths). They do not report the temperature for the next frame, probably because the flash became too dark in the frame to be analyzed. This would deny the possibility that the exposure of the first frame ended just after the very beginning of the impact phenomena and only the brief high-temperature phase was recorded in the frame. They might have observed one of the rare high-temperature-events by chance. However, it would be more probable that the time-integrated spectrum of the flash approximately consisted of the high- and low-temperature components and the observation without near-infrared wavelengths led to the high temperature.

The spectrum at the 1st frame of Flash H does not show an apparent excess in the wavelength range of less than 600 nm (Fig. 5). There are four possibilities regarding the lack of excess. First, the impact angle measured from the local horizon is smallest for the flash among the others (Table 1). Schultz (1996) found that shear heating is important in oblique impacts on particulate targets such as lunar regolith, and the amount of impact-generated vapor increases with decreasing angle while vapor temperature decreases. Radiation from a large amount of low-temperature vapor plume, including melts and dust, could have dominated this bright flash. Second, Flash H occurred near the limb of the lunar disk. Pre-existing crater rims or hills might block the radiation from the plume. Third, atmospheric scintillations could accidentally change the spectral feature. Fourth, the incomplete spectral flat-field correction for System2 described in Section 3.7 might reduce the spectral flux densities in this wavelength range.

Flash L observed by System2 does not show an apparent excess either (Supplementary figures). The atmospheric scintillation or the incomplete spectral flat-field correction could have hidden the excess. However, on the other hand, all the excesses in the spectra in Fig. 10 might be due to the atmospheric scintillations. Further spectral observations are needed to verify the existence of the excesses.

The temperatures at the 2nd and the 3rd frames (Fig. 9) are below 3000 K that is below the evaporation temperature of all silicates in Table 2 in Ahrens and O’Keefe (1972). Those after the 1st frames obtained in the NELIOTA project (Avdellidou and Vaubaillon 2019; Liakos et al., 2020) are also below 3000 K. Incandescent ejecta consisting of melts and solid particles that follows a vapor plume in a cratering process, or a radiant crater floor could be the sources of a lunar impact flash at the 2nd frame and later. Radiation probably dominated by the thermal radiation from ejecta in the latter stage was observed at the collision of the Centaur rocket with the lunar surface at  $2.5 \text{ km s}^{-1}$  (Schultz et al., 2010; Hermalyn et al., 2012). The incandescent ejecta and a crater floor observed in laboratory experiments where polycarbonate projectiles of 4.76 mm in diameter hit the quartz sand at about  $6.5 \text{ km s}^{-1}$  (Fig. 1 in Fuse et al., 2020) may simulate lunar impact flashes after the vapor plume.

Madiedo et al. (2018) reported a flash of about 7 in V-magnitude observed both at video wavelengths (no filter) and in the I-band. They assumed single blackbody radiation and calculated temperature for each set of the video- and I-band frames, and show that temperatures around 3200 K lasted for about 0.1 s after the 1st frame (frame interval of their cameras is 20 ms). However, their two video cameras were not synchronized, and probably the exposure of the no-filter camera would have

preceded the exposure of the I-band camera. Because of the decrease of brightness with time, the ratio of video wavelength brightness to I-band brightness could be larger than the real ratio. The overestimated ratios lead to higher temperatures than real temperatures. The temperatures of this flash may have been less than 3000 K as with the other results described in the previous paragraph.

Now, we consider areas radiated on the lunar surface inferred from blackbody spectra fitted to the observed spectra. There is a following relationship between the blackbody spectra  $\Phi(\lambda)$  and the Planck function  $B_T(\lambda)$  of the flash temperature  $T$ ,

$$\bar{F}_{\text{flash}}(\lambda) \cong \Phi(\lambda) = \bar{A} / r^2 \cdot B_T(\lambda) \quad (7)$$

where  $r$  is the distance to the moon and  $\bar{A}$  is the cross-sectional area of a radiating source perpendicular to the observers’ line of sight. We substituted the fitted blackbody spectrum for  $\Phi(\lambda)$  and obtained  $\bar{A}$  for the 2nd and the 3rd frames. They are listed in Table 3 as the diameters of circles that have the same area as radiating sources,  $2 \cdot \sqrt{\bar{A}/\pi}$  (effective diameter). We do not obtain the area for the 1st frames because the temperatures could be “apparent” as discussed above, and brightness would vary significantly during the exposure of the cameras. The temporal variation would be more gentle in the 2nd and the 3rd frames.

To compare with the radiating source areas, we calculated the crater diameters according to the formula for lunar craters up to roughly 100 m in diameter in loose soil or regolith developed by Gault (1974) and shown in Section 7.8 in a textbook (Melosh 1989). Impact energies, that is, the kinetic energies of meteoroids, are calculated from the masses in Table 2 and the Geminids’ impact velocity of  $35 \text{ km s}^{-1}$ . The impact angles in Table 1 are used. We used the density of meteoroids  $2.9 \times 10^3 \text{ kg m}^{-3}$  (Babadzhanov 2002) and of lunar regolith  $1.6 \times 10^3 \text{ kg m}^{-3}$  (McKay et al., 1991). These parameters result in crater diameters at the level of the pre-existing lunar surface (apparent diameters) listed in Table 3. The sizes at the 2nd frames in the table are comparable to the crater diameters; that is, the radiating source areas are comparable to the areas of crater floors. In a crater floor, only some parts would radiate. Therefore, the crater floors do not necessarily dominantly contribute to the radiation at the 2nd frames. The widespread incandescent ejecta curtain, whose effective radiating area is comparable to a crater floor area, would also be an important source. A thermally radiating spot larger than the crater size produced by the collision of the Centaur rocket with the lunar surface was observed for about 1 s after the impact before the sun illuminates the ejecta (Schultz et al., 2010). This finding also supports the idea that the coincidence of radiating sizes and crater sizes does not necessarily mean the dominance of the crater floor radiation.

## 6. Conclusions

Two simple spectral cameras at UEC recorded 13 lunar impact flashes between 6.2 and 9.9 in R-magnitude on December 15, 2018 during the Geminids meteor activity. NU and Lulin observatories separated far

**Table 3**  
Radiating source area at the 2nd and the 3rd frames.

Flash	2nd frame		3rd frame		Crater diameter/m
	T/K	size <sup>a</sup> /m	T/K	size <sup>a</sup> /m	
A	2700	3.1			4.2
B	2400	4.4	2800	1.8	7.0
G	1800	9.4			4.2
H <sup>b</sup>	2300	6.4			5.2
I	2600	5.0	2600	2.6	6.5
L	2400	2.6			5.8

<sup>a</sup> : The size (diameter) of a circle that has the same area as a radiating source.

<sup>b</sup> : Flash H was observed by System2, where the frame interval was 25 ms. The interval for the other flashes is 16 ms.

enough from UEC to discriminate lunar flashes from satellites' glints confirmed 11 of them. We derived their spectra with a time resolution of 16 ms through sophisticated procedures, such as corrections for the atmospheric dispersions and the spectral flat field. Their spectra at wavelengths between 400 nm and 870 nm are continuous and red. Best-fitted single blackbody spectra show the temperatures of about 2000–4000 K. These temperatures are almost concordant with the results obtained from multi-wavelength-band observations.

However, the composite of high (about 6000 K) and low (about 2000 K) temperature blackbody spectra could fit the observed spectra in the initial stage of a flash much better. An impact-generated optically thick vapor plume could contribute to the high-temperature component. Each part of a plume must radiate at different temperatures at a time. Furthermore, the temperature distribution in the plume must vary quickly during an exposure time for a movie frame. Nevertheless, the radiation from a part for a period may dominate the total radiation from the plume, and appears as the high-temperature component. The radiation from hot ejecta or crater floors may represent the low-temperature components. Further spectral observations are necessary to confirm the high-temperature component probably due to hot plumes.

The temperatures decrease with time, and those at the 2nd and the 3rd frames are less than 3000 K, certainly less than the evaporation temperatures of silicates. The radiating source areas at the 2nd frames are comparable to the areas of the crater floor generated by the Geminid impacts. The rough agreement does not necessarily mean that the radiant crater floors are the sources in the latter stage of the lunar impact flashes because radiating areas would be only some parts of the floors. The widespread incandescent ejecta curtain, whose effective radiating area is comparable to a crater floor area, would also be an important source.

#### CRediT authorship contribution statement

**Masahisa Yanagisawa:** Conceptualization, Methodology, Software, Validation, Investigation, Writing - original draft, Supervision, Project administration. **Yuki Uchida:** Formal analysis, Investigation, Data curation. **Seiya Kurihara:** Formal analysis, Investigation, Data curation. **Shinsuke Abe:** Investigation, Supervision. **Ryota Fuse:** Investigation. **Satoshi Tanaka:** Supervision, Project administration. **Keisuke Onodera:** Formal analysis, Investigation, Data curation. **Fumi Yoshida:** Project administration. **Hsin-Chang Chi:** Investigation, Supervision. **Zhong-Yi Lin:** Investigation, Supervision. **Jim Lee:** Investigation, Supervision. **Taichi Kawamura:** Project administration. **Ryuhei Yamada:** Project administration.

#### Declaration of competing interest

The authors declare that they have no known competing financial interests or personal relationships that could have appeared to influence the work reported in this paper.

#### Acknowledgments

We are indebted to the students of the Univ. Electro-Comm., Nihon Univ., and National Dong Hwa Univ. for their efforts in the observations. MY, SA, ST, TK, and RY were supported by the Bilateral Joint Research Program, Japan Society for the Promotion of Science, Japan. SA was supported by the Nihon University College of Science and Technology Leading Research Grant. We are greatly indebted to Prof. J. M. Madiedo and another referee for their very useful comments. MY, SA, and RF appreciate the support and hospitality of the committee members of Meteoroids (2019) held in Bratislava, Slovakia.

#### Appendix A. Supplementary data

Supplementary data to this article can be found online at <https://doi.org/10.1016/j.pss.2020.105131>.

#### References

- Abe, S., Ogawa, T., Maeda, K., Arai, T., 2020. Sodium variation in Geminid meteoroids from (3200) Phaethon. *Planet. Space Sci.* 194, 105040 <https://doi.org/10.1016/j.pss.2020.105040>.
- Ahrens, T.J., O'Keefe, J.D., 1972. Shock melting and vaporization of lunar rocks and minerals. *Moon* 4, 214–249. <https://doi.org/10.1007/BF00562927>.
- Arai, T., 41 coauthors, 2018. DESTINY+ mission: Flyby of Geminids parent asteroid (3200) Phaethon and in-situ analyses of dust accreting on the earth. In: 49th Lunar and Planetary Science Conference, Abstract No. 2570.
- Artemieva, N.A., Shuvalov, V.V., Trubetskaya, I.A., 2000. Lunar leonid meteors - Numerical simulations. 31th Lunar and Planetary Science Conference, Abstract No. 1402.
- Avdellidou, C., Vaubaillon, J., 2019. Temperatures of lunar impact flashes: mass and size distribution of small impactors hitting the moon. *Mon. Not. Roy. Astron. Soc.* 484, 5212–5222. <https://doi.org/10.1093/mnras/stz355>.
- Babadzhanov, P.B., 2002. Fragmentation and densities of meteoroids. *Astron. Astrophys.* 384, 317–321. <https://doi.org/10.1051/0004-6361/20020010>.
- Beech, M., 2002. The age of the Geminids: a constraint from the spin-up time-scale. *Mon. Not. Roy. Astron. Soc.* 336, 559–563. <https://doi.org/10.1046/j.1365-8711.2002.05778.x>.
- Bellot Rubio, L.R., Ortiz, J.L., Sada, P.V., 2000a. Luminous efficiency in hypervelocity impacts from the 1999 Lunar Leonids. *Astrophys. J.* 542, L65–L68. <https://doi.org/10.1086/312914>.
- Bellot Rubio, L.R., Ortiz, J.L., Sada, P.V., 2000b. Observation and interpretation of meteoroid impact flashes on the moon. *Earth Moon Planets* 82–83, 575–598. <https://doi.org/10.1023/A:1017097724416>.
- Bessell, M.S., 2005. Standard photometric systems. *Annu. Rev. Astron. Astrophys.* 43, 293–336. <https://doi.org/10.1146/annurev.astro.41.082801.100251>.
- Bonanos, A.Z., Avdellidou, C., Liakos, A., Xilouris, E.M., Dapergolas, A., Koschny, D., Bellas-Velidis, I., Boumis, P., Charmandaris, V., Fytsilis, A., Maroussis, A., 2018. NELIOTA: first temperature measurement of lunar impact flashes. *Astron. Astrophys.* 612 (A76), 6. <https://doi.org/10.1051/0004-6361/201732109>.
- Cooke, W.J., Suggs, R.M., Suggs, R.J., Swift, W.R., Hollon, N.P., 2007. Rate and distribution of kilogram lunar impactors. 38th Lunar and Planetary Science Conference, Abstract No. 1986.
- Ernst, C.M., Schultz, P.H., 2002. Effect of velocity and angle on light intensity generated by hypervelocity impacts. 33th Lunar and Planetary Science Conference, Abstract No. 1782.
- Ernst, C.M., Schultz, P.H., 2004. Early-time temperature evolution of the impact flash and beyond. 35th Lunar and Planetary Science Conference, Abstract No. 1721.
- Ernst, C.M., Schultz, P.H., 2007. Evolution of the Deep Impact flash: implications for the nucleus surface based on laboratory experiments. *Icarus* 190, 334–344. <https://doi.org/10.1016/j.icarus.2007.03.030>.
- Flower, P.J., 1996. Transformations from theoretical Hertzspring-Russell diagrams to color-magnitude diagrams: effective temperatures, B-V colors, and bolometric corrections. *Astrophys. J.* 469, 355–365. <https://doi.org/10.1086/177785>.
- Fuse, R., Abe, S., Yanagisawa, M., Hasegawa, S., 2020. An experimental study of the impact flash: the relationship between luminous efficiency and vacuum level. *Planet. Space Sci.* 187, 104921 <https://doi.org/10.1016/j.pss.2020.104921>.
- Gault, D.E., 1974. Impact cratering. In: Greeley, R., Schultz, P.H. (Eds.), *A Primer in Lunar Geology*. NASA Ames, pp. 137–175.
- Hermalyn, B., Schultz, P.H., Shirley, M., Ennico, K., Colaprete, A., 2012. Scouring the surface: ejecta dynamics and the LCROSS impact event. *Icarus* 218, 654–665. <https://doi.org/10.1016/j.icarus.2011.12.025>.
- Jewitt, D., Hsieh, H., Agarwal, J., 2015. The active asteroids. In: Michel, P., DeMeo, F.E., Bottke, W.F. (Eds.), *Asteroids IV*. Univ. Arizona Press, Tucson, pp. 221–241. [https://doi.org/10.2458/azu\\_uapress.9780816532131-ch012](https://doi.org/10.2458/azu_uapress.9780816532131-ch012).
- Kasuga, T., Jewitt, D., 2019. Asteroid-Meteoroid Complexes. In: Ryabova, G.O., Asher, D.J., Campbell-Brown, M.D. (Eds.), *Meteoroids*. Cambridge Univ. Press, pp. 187–209. <https://doi.org/10.1017/9781108606462>.
- Kurosawa, K., Kadono, T., Sugita, S., Shigemori, K., Sakaiya, T., Hironaka, Y., Ozaki, N., Hiroshita, A., Cho, Y., Tachibana, S., Vinci, T., Ohno, S., Kodama, R., Matsui, T., 2012a. Shock-induced silicate vaporization: the role of electrons. *J. Geophys. Res.* 117 (E4), 14. <https://doi.org/10.1029/2011JE004031>.
- Kurosawa, K., Ohno, S., Sugita, S., Mieno, T., Matsui, T., Hasagawa, S., 2012b. The nature of shock-induced calcite (CaCO<sub>3</sub>) devolatilization in an open system investigated using a two-stage light gas gun. *Earth Planet. Sci. Lett.* 337–338, 68–76. <https://doi.org/10.1016/j.epsl.2012.05.022>.
- Liakos, A., Bonanos, A., Xilouris, E., Bellas-Velidis, I., Boumis, P., Charmandaris, V., Dapergolas, A., Fytsilis, A., Maroussis, A., Koschny, D., Moissl, R., Navarro, V., January 2019. NELIOTA lunar impact flash detection and event validation. In: *Proceedings of the "ESA NEO and Debris Detection Conference - Exploiting Synergies held in ESA/ESOC, Darmstadt, Germany*, pp. 22–24.
- Liakos, A., Bonanos, A.Z., Xilouris, E.M., Koschny, D., Bellas-Velidis, I., Boumis, P., Charmandaris, V., Dapergolas, A., Fytsilis, A., Maroussis, A., Moissl, R., 2020. NELIOTA: methods, statistics, and results for meteoroids impacting the moon. *Astron. Astrophys.* 633 (A112), 29. <https://doi.org/10.1051/0004-6361/201936709>.
- Madiedo, J.M., Ortiz, J.L., Yanagisawa, M., Aceituno, J., Aceituno, F., 2019a. Impact Flashes of Meteoroids on the Moon. In: Ryabova, G.O., Asher, D.J., Campbell-Brown, M.D. (Eds.), *Meteoroids*. Cambridge Univ. Press, pp. 136–158. <https://doi.org/10.1017/9781108606462>.
- McKay, D.S., Heiken, G., Basu, A., Blanford, G., Simon, S., Reedy, R., French, B.M., Papike, J., 1991. *The Lunar Regolith*. In: Heiken, G.H., Vaniman, D.T., French, B.M. (Eds.), *Lunar Source Book*. Cambridge Univ. Press, pp. 285–356.

- Madiedo, J.M., Ortiz, J.L., Morales, N., 2018. The first observations to determine the temperature of a lunar impact flash and its evolution. *Mon. Not. Roy. Astron. Soc.* 480, 5010–5016. <https://doi.org/10.1093/mnras/sty1862>.
- Madiedo, J.M., Ortiz, J.L., Morales, N., Román, A., Alonso, S., 2019c. Lunar impact flashes recorded during the 2018 Geminids: preliminary results. 50th lunar and planetary science conference, abstract No. 1406.
- Madiedo, J.M., Ortiz, J.L., Morales, N., Santos-Sanz, P., 2019b. Multiwavelength observations of a bright impact flash during the January 2019 total lunar eclipse. *Mon. Not. Roy. Astron. Soc.* 486, 3380–3387. <https://doi.org/10.1093/mnras/stz932>.
- Melosh, H.J., 1989. *Impact Cratering: A Geologic Process*. Oxford Univ. Press, New York. <https://doi.org/10.1017/S0016756800007068>.
- Moser, D.E., Suggs, R.M., Swift, W.R., Suggs, R.J., Cooke, W.J., Diekmann, A.M., Koehler, H.M., 2010. Luminous efficiency of hypervelocity meteoroid impacts on the moon derived from the 2006 Geminids, 2007 Lyrids, and 2008 Taurids. *Proceedings of the Meteoroids 2010 Conference*. 142–154. In: NASA CP-2011-216469.
- Nemtchinov, I.V., Shuvalov, V.V., Artemieva, N.A., Ivanov, B.A., Kosarev, I.B., Trubetskaya, I.A., 1998a. Light flashes caused by meteoroid impacts on the lunar surface. *Sol. Syst. Res.* 32, 99–114.
- Nemtchinov, I.V., Shuvalov, V.V., Artemieva, N.A., Ivanov, B.A., Kosarev, I.B., Trubetskaya, I.A., 1998b. Light impulse created by meteoroids impacting the moon. 29th Lunar and Planetary Science Conference, Abstract No. 1032.
- Ortiz, J.L., Madiedo, J.M., Morales, N., Santos-Sanz, P., Aceituno, F.J., 2015. Lunar impact flashes from Geminids: analysis of luminous efficiencies and the flux of large meteoroids on Earth. *Mon. Not. Roy. Astron. Soc.* 454, 344–352. <https://doi.org/10.1093/mnras/stv1921>.
- Ramírez, I., Michel, R., Sefako, R., Tucci Maia, M., Schuster, W.J., van Wyk, F., Meléndez, J., Casagrande, L., Castilho, B.V., 2012. The UBV(RI)<sub>C</sub> colors of the sun. *Astrophys. J.* 752, 12. <https://doi.org/10.1088/0004-637X/752/1/5>.
- Schubert, G., Walterscheid, R.L., 1999. Earth. In: Cox, A.N. (Ed.), *Allen's Astrophysical Quantities*, fourth ed. Springer, New York, pp. 239–292.
- Schultz, P.H., 1996. Effect of impact angle on vaporization. *J. Geophys. Res.* 101 (E9), 21117–21136. <https://doi.org/10.1029/96JE02266>.
- Schultz, P.H., Eberhardy, C.A., Ernst, C.M., A'Hearn, M.F., Sunshine, J.M., Lisse, C.M., 2007. The Deep Impact oblique impact cratering experiment. *Icarus* 190, 295–333. <https://doi.org/10.1016/j.icarus.2007.06.006>.
- Schultz, P.H., Hermalyne, B., Colaprete, A., Ennico, K., Shirley, M., Marshall, W.S., 2010. The LCROSS cratering experiment. *Science* 330, 468–472. <https://doi.org/10.1126/science.1187454>.
- Schultz, P.H., Eberhardy, C.A., 2015. Spectral probing of impact-generated vapor in laboratory experiments. *Icarus* 248, 448–462. <https://doi.org/10.1016/j.icarus.2014.10.041>.
- Sugita, S., Schultz, P.H., Adams, M.A., 1998. Spectroscopic measurement of vapor clouds due to oblique impacts. *J. Geophys. Res.* 103, 19,427–19,441. <https://doi.org/10.1029/98JE02026>.
- Sugita, S., Schultz, P.H., 1999. Spectroscopic characterization of hypervelocity jetting: comparison with a standard theory. *J. Geophys. Res.* 104, 30,825–30,845. <https://doi.org/10.1029/1999JE001061>.
- Sugita, S., Schultz, P.H., Hasegawa, S., 2003. Intensities of atomic lines and molecular bands observed in impact-induced luminescence. *J. Geophys. Res.* 108 (E12), 14. <https://doi.org/10.1029/2003JE002156>.
- Suggs, R.M., Moser, D.E., Cooke, W.J., Suggs, R.J., 2014. The flux of kilogram-sized meteoroids from lunar impact monitoring. *Icarus* 238, 23–26. <https://doi.org/10.1016/j.icarus.2014.04.032>.
- Szalay, J.R., Pokorný, P., Jenniskens, P., Horányi, M., 2018. Activity of the 2013 Geminid meteoroid stream at the moon. *Mon. Not. Roy. Astron. Soc.* 474, 4225–4231. <https://doi.org/10.1093/mnras/stx3007>.
- Tang, E., Shi, X., Zhang, Q., Wang, M., Wang, D., Xiang, S., Liu, S., Xia, J., He, L., Han, Y., 2015. Characterization of light flash signatures using optical-fiber pyrometer detectors during hypervelocity impact. *Int. J. Appl. Electromagn. Mech.* 47, 513–521. <https://doi.org/10.3233/JAE-140015>.
- Vaubailion, J., Neslusan, L., Sekhar, A., Rudawska, R., Ryabova, G.O., 2019. From Parent Body to Meteor Shower: The Dynamics of Meteoroid Streams. In: Ryabova, G.O., Asher, D.J., Campbell-Brown, M.D. (Eds.), *Meteoroids*. Cambridge Univ. Press, pp. 161–186. <https://doi.org/10.1017/9781108606462>.
- Xilouris, E.M., Bonanos, A.Z., Bellas-Velidis, I., Boumis, P., Dapergolas, A., Maroussis, A., Liakos, A., Alikakos, I., Charmandaris, V., Dimou, G., Fytsilis, A., Kelley, M., Koschny, D., Navarro, V., Tsiganis, K., Tsinganos, K., 2018. NELIOTA: the wide-field, high-cadence, lunar monitoring system at the prime focus of the Kryoneri telescope. *Astron. Astrophys.* 619 (A141), 14. <https://doi.org/10.1051/0004-6361/201833499>.
- Yamada, R., Garcia, R.F., Lognonné, P., Le Feuvre, M., Calvet, M., Gagnepain-Beyneix, J., 2011. Optimisation of seismic network design: application to a geophysical international lunar network. *Planet. Space Sci.* 59, 343–354. <https://doi.org/10.1016/j.pss.2010.12.007>.
- Yamada, R., Kawamura, T., Yanagisawa, M., Abe, S., Fukuhara, T., Onodera, K., Uchida, Y., Kurihara, S., Fuse, R., Yoshida, F., Chi, H., Avdellidou, C., Shirai, K., Ishihara, Y., Tanaka, S., Shiraishi, H., Wiczoreck, M., 2019. The international observation of lunar impact flashes and application of the results to future lunar seismic experiments. 50th Lunar and Planetary Science Conference, Abstract No. 1770.
- Yanagisawa, M., Kisaichi, N., 2002. Lightcurves of 1999 Leonid impact flashes on the moon. *Icarus* 159, 31–38. <https://doi.org/10.1006/icar.2002.6931>.
- Yanagisawa, M., Ikegami, H., Ishida, M., Karasaki, H., Takahashi, J., Kinoshita, K., Ohnishi, K., 2008. Lunar impact flashes by Geminid meteoroids. In: 2007. 71st Annual Meteoritical Society Meeting, Meteoritics and Planetary Sciences Supplement 43, Id. 5169.